Towards functionalization of graphene: *in situ* study of the nucleation of copper-phtalocyanine on graphene

2016 New J. Phys. 18 023034

(http://iopscience.iop.org/1367-2630/18/2/023034)

New Journal of Physics
The open access journal at the forefront of physics

Deutsche Physikalische Gesellschaft DPG
IOP Institute of Physics

Published in partnership with: Deutsche Physikalische Gesellschaft and the Institute of Physics

OPEN ACCESS

RECEIVED
9 September 2015

REVISED
27 November 2015

ACCEPTED FOR PUBLICATION
4 January 2016

PUBLISHED
8 February 2016

PAPER

Towards functionalization of graphene: *in situ* study of the nucleation of copper-phtalocyanine on graphene

Daniel Schwarz[1], **Caroline Henneke and Christian Kumpf**

Peter Grünberg Institut (PGI-3), Forschungszentrum Jülich, D-52425 Jülich and JARA-Fundamentals of Future Information Technologies (JARA-FIT), Germany

[1] *Present address*: Advanced Light Source, Lawrence Berkeley Laboratory, Berkeley 94720, USA.

E-mail: c.kumpf@fz-juelich.de

Keywords: low energy electron microscopy (LEEM), graphene functionalization, nucleation and growth, graphene films, molecular films, thin film growth

Abstract

Molecular films present an elegant way for the uniform functionalization or doping of graphene. Here, we present an *in situ* study on the initial growth of copper phthalocyanine (CuPc) on epitaxial graphene on Ir(111). We followed the growth up to a closed monolayer with low energy electron microscopy and selected area electron diffraction (μLEED). The molecules coexist on graphene in a disordered phase without long-range order and an ordered crystalline phase. The local topography of the graphene substrate plays an important role in the nucleation process of the crystalline phase. Graphene flakes on Ir(111) feature regions that are under more tensile stress than others. We observe that the CuPc molecules form ordered domains initially on those graphene regions that are closest to the fully relaxed lattice. We attribute this effect to a stronger influence of the underlying Ir(111) substrate for molecules adsorbed on those relaxed regions.

1. Introduction

A wide range of applications for graphene has been proposed following the isolation of individual monolayer sheets by Geim in 2005 [1]. These applications include the use of graphene as a transparent electrode material for organic light emitting diodes or organic photovoltaics [2–5], as a growth modifier for organic crystals [6–8], in single molecule sensors [9–11], or as a replacement of silicon in future high performance electronics [12]. All of these applications require some means of functionalization of the pristine graphene sheets, either simply for electronic contacting or to alter its properties as needed, e.g., to induce a band gap for the use in a field effect transistor. One possible way to achieve this is surface functionalization with adsorbates [13–17]. Ideally, the adsorbates should be adsorbed at well defined lattice sites on the graphene surface and in a regular way, to keep the full symmetry and thus properties of the honeycomb graphene lattice. This is a challenge, since due to graphene's inertness, the surface energy of most materials on graphene is rather small. As a result most materials are not growing as smooth films on graphene but rather as clusters.

A viable strategy for functionalization could be the modification with adsorbed molecules [13–15, 18–20]. The molecules can be deposited on the graphene surface using wet chemistry or vapor deposition techniques. It is possible to induce and tune an energy band gap and dope graphene by adsorption of molecules [19].

Phtalocyanines represent a particularly appealing class of molecules for graphene functionalization, since they consist of an organic frame and a metal center atom that can be, for example, Cu, Sn, Zn, Fe or Al. Phtalocyanines often form regular superstructures on graphene, which opens up the possibility to bring metal centers with different functionality to specific sites on the graphene lattice [6–8, 21–26]. Understanding and controlling the crystallization of these molecules on graphene is important to create the functionalization that is desired.

Here, we present a study on the initial growth of copper-phtalocyanine (CuPc) molecular films on epitaxial graphene. We followed the deposition of CuPc molecules on graphene it in-situ using low-energy electron

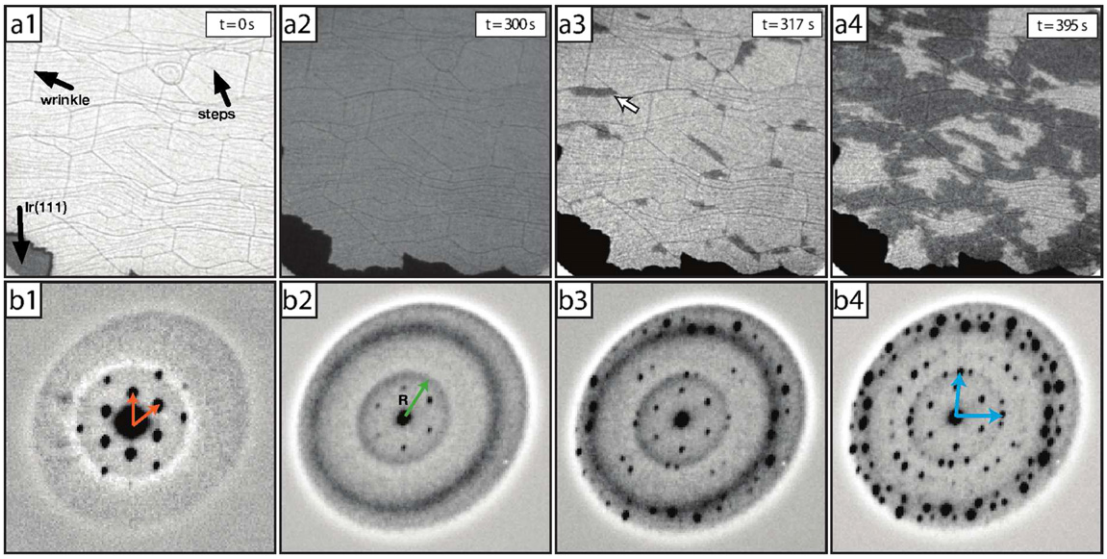

Figure 1. (a1)–(a4) Bright field LEEM image sequence of the deposition of CuPc. The field of view (FOV) is 10 μm, the start voltage is 1.8 V. The black arrows in the first image (a1) point at Ir steps (thin lines), graphene wrinkles (thick lines) and the Ir(111) substrate (dark gray). The white arrow in the third image ((a3), $t = 317$ s) points at a crystalline CuPc domain. The times in the images refer to opening the shutter of the CuPc evaporator. (b1)–(b4) μLEED patterns obtained in a separate experiment at similar conditions (start voltage 6 V). The orange arrows in the first pattern (b1) represent the unit cell in reciprocal space of the graphene Moiré pattern, the first order Ir(111) spots are *not* visible as they are outside the Ewald sphere. The Moiré pattern does not change during CuPc adsorption. The blue arrows in the fourth pattern (b4) indicate the unit cell of one of the CuPc domains.

microscopy (LEEM) and selected area low-energy electron diffraction (μLEED). The first technique allows to follow the growth of molecular layers at submonolayer coverages with high spatial resolution (down to 2 nm) while the second enables the structural analysis, both at varying substrate temperature in a large field of view. The influence of substrate defects, e.g., steps or point defects, on the growth process becomes immediately apparent. This makes LEEM a powerful tool to investigate the growth of molecular thin films [5, 27–36].

As a substrate we choose epitaxial graphene on Ir(111), grown through the decomposition of ethylene gas at elevated temperatures on the Ir surface [37, 38]. In this way, it is possible to obtain large individual graphene flakes of highest quality. The weak interaction of graphene with the Ir(111) substrate expresses itself in a slight p-doping [23, 39]. The mismatch between the Ir(111) and graphene lattice results in a Moire pattern with a weak corrugation, that was used before for the selective adsorption of metal clusters or FePc molecules [26, 38, 40].

In this paper we report on our study of the nucleation, growth and structure of an ordered, crystalline CuPc film that forms at CuPc coverages close to a full monolayer. We show that the nucleation and growth of domains (crystallites) of the crystalline film is strongly influenced by the local topography of the graphene sheet and the local alignment of the graphene lattice w.r.t. the underlying Ir(111) substrate.

2. Experimental

The experiments were performed in an Elmitec LEEM III low energy electron microscope. The instrument is aberration corrected with a lateral resolution down to 2.0 nm. The microscope also allows to obtain electron diffraction patterns from selected areas of less than 1 μm diameter on the surface (μLEED).

An Ir(111) single crystal was prepared by repeated cycles of sputtering with argon (1 kV), heating in oxygen (1×10^{-8} mbar) at approximately 850 K and flashing to >1400 K in UHV. Epitaxial graphene was grown through chemical vapor deposition by cracking of ethylene molecules at the surface [37, 38, 41]. The growth recipe we used was as follows: we admitted small amounts of ethylene to a total pressure of 5×10^{-9} mbar, while keeping the substrate temperature constant at around 1300 K. We monitored the growth of graphene flakes in LEEM until a major fraction of the surface was covered with sufficiently large single crystal graphene flakes (exceeding 10 μm in diameter, see figure 1(a)). At this point the ethylene gas was pumped off and the crystal kept at high temperature for a short time to allow residual carbon to attach to graphene flakes. Next, the crystal was cooled using liquid nitrogen to the temperatures used for the subsequent CuPc growth experiments (between 220 and 340 K). For each growth experiment we cleaned the Ir(111) surface using the same procedure

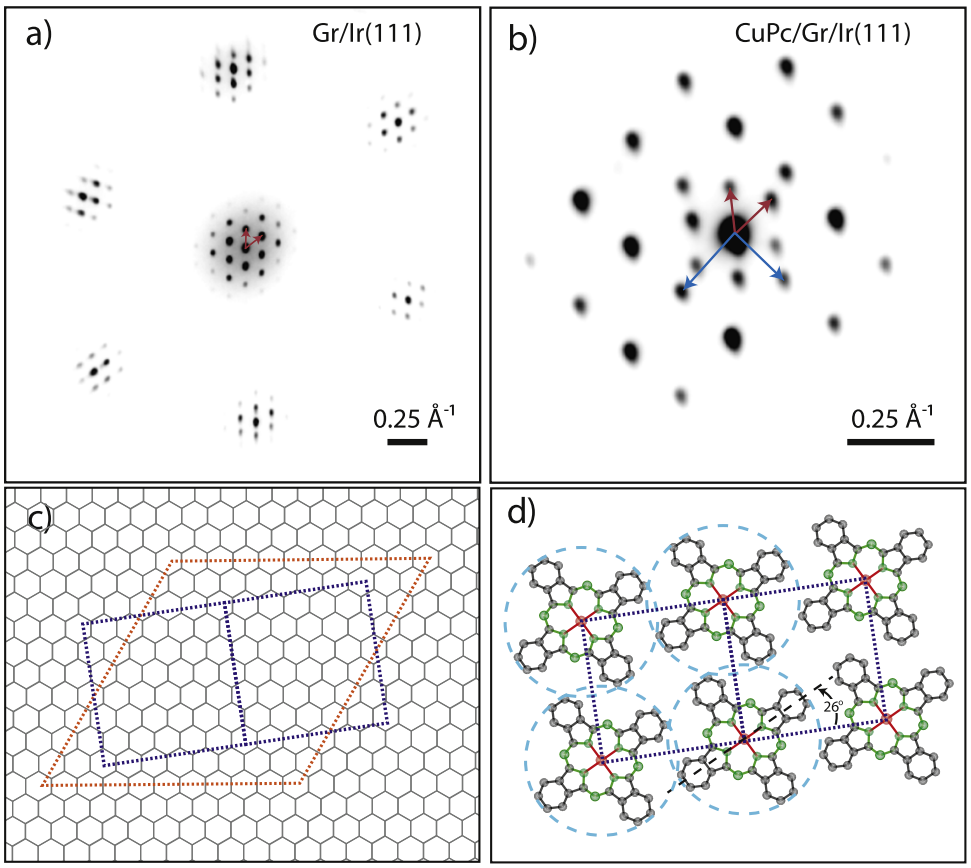

Figure 2. (a) μLEED pattern from a pristine R0 graphene flake aligned with the Ir(111) substrate. LEED patterns from 30 to 120 V in 1 V steps were summed up to obtain a cumulative pattern. Dark red arrows here (and in (b)) indicate the unit cell of the Moiré superstructure [38]. (b) Diffraction pattern (cumulative pattern from 2.0 to 10.0 V in 0.1 V steps) obtained from an individual CuPc domain using an illumination aperture. The pattern shows a square CuPc unit cell (blue arrows) with a lattice constant of 1.38 ± 0.04 nm, rotated by about 9° w.r.t. the underlying Moiré pattern. In total we find six equivalent rotational CuPc domains. (c) Schematic of the Moiré unit cell, (orange dashed parallelogram) and the CuPc unit cell (dark blue square), drawn on top of the graphene lattice. Note, that we cannot determine the CuPc adsorption sites from the diffraction pattern. (d) Sketch of the CuPc unit cell. The light blue dashed circles indicate the CuPc van der Waals diameter of freely rotating molecules for comparison. Black circles represent carbon, green nitrogen and red copper atoms.

and prepared fresh graphene flakes. The recipe results in large flakes, but of varying orientation with respect to the underlying Ir(111) substrate [42]. Therefore, we checked the crystallographic orientation of the graphene flakes prior the experiments using μLEED (see figure 2(a))[2].

Graphene forms different rotational domains on Ir(111) [43]. With the above mentioned growth recipe the majority of graphene flakes is aligned with the Ir(111) substrate (R0 flakes). The second most abundant orientations are R30 and R14.4. If not mentioned otherwise, we observed the CuPc on R0 flakes, as confirmed with μLEED.

Deposition was performed by evaporating CuPc from a home-made resistively heated Knudsen cell. Evaporation rates of approximately $2–3 \times 10^{-3}$ ML s^{-1} were used, calibrated by the time needed to obtain a full, ordered monolayer (ML) in LEEM. We define one monolayer as the density of molecules adsorbed to fully cover the surface with a single layer.

If not otherwise stated, we collected LEEM images using start voltages between 2.4 and 3.0 V in bright field mode. We did not observe any electron beam induced damage of the molecular films under the imaging conditions described here. However, at slightly higher start voltages (>8 V) we did observe severe damage to the films and increased mobility of the molecules. We tried to avoid these energies during the experiments. If unavoidable (e.g. for μLEED experiments), we minimized the electron dose and moved to a new position on the sample for further experiments.

[2] Note that LEED patterns recorded in a LEEM instrument have a constant k-space scaling, i.e., diffractions spots do not change their positions in the image when the electron energy is changed. This is due to the electron optics being operated at very high voltages (20 kV in our case).

3. Growth of the first layer

3.1. Different growth stages

First, we describe the different stages of the growth and structure of the first CuPc molecular layer. Understanding the factors that influence the growth of the first layer is crucial, since it is this layer that will be governing both the electronic interaction with the underlying graphene, as well as the crystalline structure (molecule orientation, grain density) of thicker CuPc films.

Figure 1(a) shows a (bright field) LEEM image sequence of the deposition of CuPc at a substrate temperature of about 220 K. The sample temperature is measured with a C type thermocouple and the absolute error at these low temperatures is relatively large. The sequence starts with an image of the pristine graphene substrate *before* opening the shutter of the CuPc evaporator (figure 1(a1)). The three arrows point at wrinkles in the graphene layer [41], underlying Ir steps and the bare Ir(111) substrate, respectively. Under the imaging conditions used here, the graphene flake appears brighter than the Ir substrate.

The next image in the sequence (figure 1(a2)) shows the same flake 300 s *after* opening the shutter of the CuPc evaporator (at $t = 0$ s). The CuPc coverage at this point is about 0.7–0.8 ML. After opening the shutter, the image intensity of both the graphene flake and the bare Ir(111) decreased homogeneously over the whole surface with increasing deposition time (see figure 1(a2)). We attribute this to the presence of adsorbed CuPc molecules in a disordered phase on the surface as it was observed for CuPc and SnPc adsorption on different metal substrates [44–47]. A combination of two mechanisms explains the reduced image intensity: (1) molecules scatter the probing electrons out of the specular direction [31, 48–51], and (2) destructive interference between electrons reflected from the molecular adlayer and the graphene substrate. The presence of the disordered phase is also confirmed by the observation of a diffraction ring in μLEED experiments (figure 1(b2)), which were recorded under comparable conditions in a separate experiment. The radius of the ring (green arrow, $R = 0.41$ Å^{-1}) corresponds to a preferred intermolecular distance (1.53 nm for the image shown), which in turn is compatible with a coverage of 0.81 ML.

Once the adsorbed CuPc molecules were sufficiently dense, we observed the nucleation of domains of an ordered CuPc phase (see figure 1(a3), $t = 317$ s). Domains of this phase nucleate preferably at graphene wrinkles, which suggest defect induced nucleation (heteronucleation). Upon further deposition of CuPc these domains expand and new domains continue to nucleate (figure 1(a4)). Micro diffraction patterns taken from these domains reveal a highly ordered, square crystal structure (figure 1(b4)). Eventually the whole surface is covered with this ordered phase, after which a second layer would nucleate. In the μLEED patterns (figures 1(b3) and (b4)), we can see that the rings of the disordered phase almost completely disappear and sharp spots develop, as the CuPc coverage increases and a larger fraction of the surface is covered with the crystalline phase.

From the diameter of the diffuse diffraction ring just before nucleation, we can extract the density of adsorbed molecules necessary for nucleation of the crystalline phase at this temperature. However, before we do that and further discuss the nucleation mechanism in detail, we will first analyze the diffraction pattern of the ordered phase and the crystalline structure in the first monolayer.

3.2. Structure of the first CuPc layer

In the previous section we showed that two distinct submonolayer phases are formed by CuPc on graphene: a disordered phase for low coverages and a 2D crystalline phase for higher coverages close to a full monolayer. To determine the molecular structure within the crystalline phase, we obtained μLEED patterns from individual domains. A μLEED pattern of the pristine (uncovered) graphene flake is shown in figure 2(a). The six first order Ir(111) diffraction spots are surrounded by several satellite spots. These originate from the well known Moiré pattern formed by the graphene overlayer and the Ir(111) substrate lattice [37–40]. The period length of this Moiré pattern was measured to be 2.55 nm at temperatures below 500 K using high resolution LEED [41]. This period length is not altered by the adsorption of the weakly interacting CuPc molecules. We determined the positions of the CuPc diffraction spots relative to these Moiré spots, which allowed us to stay below the electron energies where electron induced damage starts to become a problem (approximately 6–8 V).

The μLEED pattern shown in figure 1(b4) is a superposition of several different rotational CuPc domains. To determine the CuPc unit cell we obtained diffraction patterns from individual rotational domains using an illumination aperture producing a 500 nm diameter illuminated spot on the surface. An example of such a LEED pattern is shown in figure 2(b). We find a square unit cell (taking into account an instrument induced distortion of the LEED pattern), with a lattice constant of 1.38 ± 0.04 nm. This value is very close to the lattice constant of bulk CuPc layers on HOPG [52]. The unit vectors make an angle of about 9°, and 39°with respect to the underlying Moiré pattern (and thus with the aligned graphene and the [1 $\bar{1}$ 0] Ir substrate direction).

Figures 2(c) and (d) illustrate the proposed molecular structure in the crystalline first layer. From what is known for the adsorption of CuPc on graphene, graphite and metal surfaces, it is reasonable to assume that the

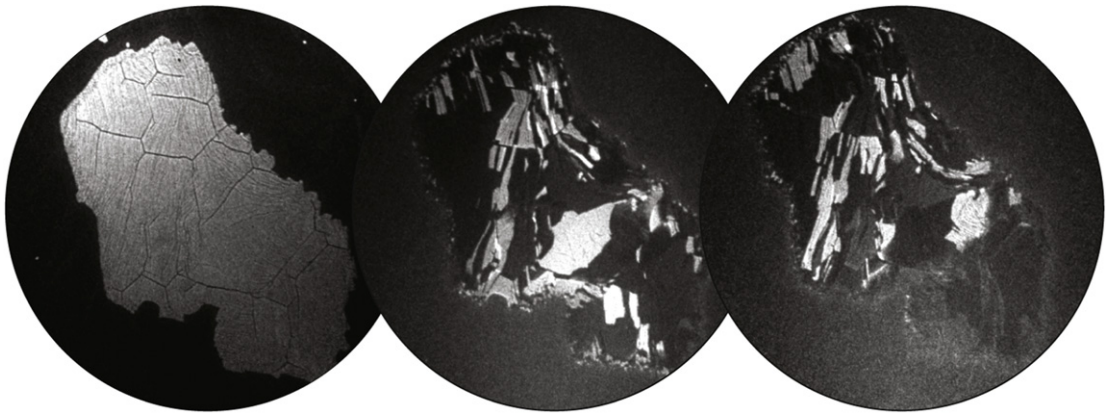

Figure 3. Bright and dark field LEEM images of a closed CuPc monolayer grown at approximately 210 K. Left: bright field LEEM with an FoV of 10 μm and an start voltage of 1.7 V. Middle and right: dark field LEEM images using one of the first order CuPc diffraction spots (see figure 2), start voltage is 3.1 V. Areas with the same brightness level have identical rotational crystal orientation.

molecules adsorb in a flat lying geometry at all times [7, 45–47, 53–59]. Figure 2(c) shows the CuPc unit cell on the graphene substrate together with the Moire unit cell. In our model the molecules form an angle of about 26° with the superstructure unit cell vector, see figure 2(d). The structure is very similar to the structure of CoPc on graphene/Ir(111) [21]. Unlike for the case of FePc on graphene/Ru(0001) [60], there is no indication that the Moiré pattern is trapping the CuPc molecules in fixed positions. However, while the CuPc structure is incommensurate w.r.t. the underlying graphene and Ir substrate, the substrate symmetry is still imposed on the CuPc layer. In accordance with the substrate symmetry, we observed in total six rotational CuPc domains.

From dark field LEEM, i.e., imaging by selecting a diffraction spot with a contrast aperture, we find that individual rotational CuPc domains can extend over micrometers in size (see figure 3). This shows that each individual nuclei that formed during nucleation is a single crystal, which implies a high crystal quality and minimum grain density. While underlying Ir(111) steps sometimes block the domain expansion, we never observed the growth of a domain over a wrinkle in the graphene layer. The maximum size (and thus the grain density) of individual crystallites is thus only limited by graphene wrinkles.

3.3. Details of the phase transformation

For sub-monolayer coverages the CuPc molecules form a phase without long range order. We can discern two discrete rings in the diffraction pattern of the dilute phase (figure 1(b2)). These two rings are *not* first and second order diffraction rings [46, 47]. The inner (and less intense) ring is due to *intermolecular* diffraction, i.e., is showing the average separation of molecules. As expected, this ring is changing in diameter with coverage. The outer (and more intense) diffraction ring, on the other hand, is due to *intramolecular* diffraction. This ring is not changing in diameter with CuPc coverage.

From the diameter of the inner diffraction ring in figure 1(b2) we can roughly determine the average separation d between molecules and, assuming a random spatial distribution of molecules, their density $n = 1/d^2$. We find that the average separation between molecules just before nucleation of the crystalline phase is close to 1.53 $\pm$ 0.03 nm. This separation is just slightly larger than the projected van der Waals diameter of a single CuPc molecule adsorbed in a flat geometry (1.49 nm [45]). There is no intensity modulation visible in both diffraction rings, i.e., there is no strongly preferred molecular orientation in the disordered phase. The surface just before nucleation of the crystalline phase is occupied by randomly oriented molecules. From the mean separation of 1.53 nm follows a CuPc density of 81% of the density in the crystalline phase, or 0.81 ML (according to our definition of a monolayer as a fully closed layer of the crystalline phase). This value is the CuPc density needed for nucleation at a substrate temperature of 220 K.

For higher temperatures, we find that an even denser disordered phase is necessary to induce nucleation. Figure 4 shows the melting of CuPc domains upon increasing the substrate temperature from the growth temperature of 220 K. The molecules leave the crystalline phase and stay on the surface in the disordered phase. Close to room temperature almost all the CuPc domains have melted. Note, that this temperature depends on the total coverage[3], i.e., for a higher total coverage the domains would melt at a higher temperature. In fact, a closed monolayer is stable up to approximately 450 K. Upon cooling the substrate the crystalline domains reappear. It is remarkable that the domains form again at almost identical places, due to the influence of the

[3] Total coverage is the sum of the adsorbed molecules in the (coexisting) disordered and ordered phases.

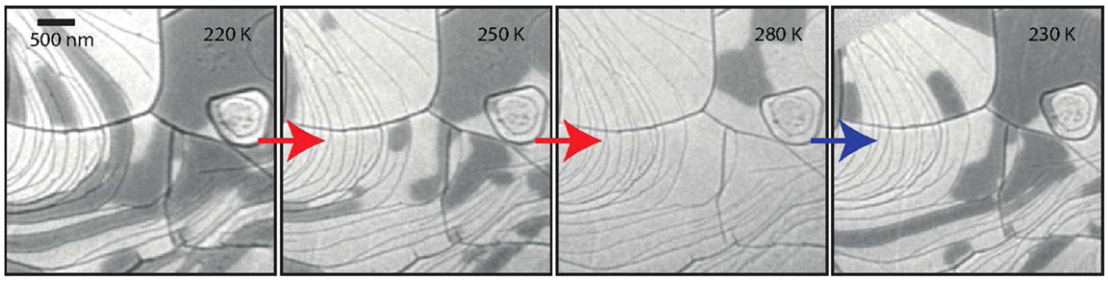

Figure 4. Heating and cooling of a graphene flake partially covered with CuPc domains (dark gray). The total CuPc coverage is 0.92 ML. Upon increasing the temperature the CuPc domains melt. In the third image close to room temperature almost all CuPc domains have vanished. Upon cooling down again the domains reappear.

topography, as discussed in the next section. From the images, we judge that the amount of molecules desorbing from the flake is negligible and therefore the melting process is reversible.

In our experiment the disordered phase covered about 40% of the surface at a density of 81% of a closed layer and at 220 K, while the rest is covered with the 2D crystalline phase. At 280 K the disordered phase covers 90% of the surface. Assuming no desorption of molecules, this means that the disordered phase now has a density of 87% of a closed layer. Unfortunately the temperature measurement is neither accurate nor precise enough for a full analysis of this phase transformations and extraction of thermodynamic parameters.

Apparently, the crystallization of the CuPc molecules is a first order phase transition. It is often intuitively assumed, that this transition is caused by attractive molecule–molecule interaction, e.g., by overcoming the orientational and translational entropy of the disordered phase by decreasing the internal energy through the formation of bonds. However, one very general class of first order phase transitions is purely entropy driven. One of such systems, namely non-interacting hard disks in two-dimensions, has been studied extensively theoretically in the last decades—and is still not fully understood [61–65]. This system can be seen as a simplified model of our system of adsorbed CuPc molecules (an even more accurate description are non-interacting hard squares, which is, however, less frequently studied [64, 66]). Indeed, the hard disk model also has a first order phase transition at a packing factor of 0.723. This value is very close to the nucleation density of CuPc at 220 K (the aforementioned CuPc coverage of 0.81 ML at 220 K translates into a packing factor of 0.735). However, the hard disk system is independent of temperature, which only sets the time scale. We, however, observed reversible melting/crystallization upon changing the substrate temperature, which can only be explained by the presence of internal energy, i.e., attractive molecule–molecule interaction. Interestingly, we observe densities in the disordered phase that exceed by far the critical packing factor of 0.723 of the hard disk model, even taking into account measurement errors. This is very counter intuitive, but might be explained by an average attractive molecule–molecule interaction term in the disordered phase, which is stabilizing a denser packing.

4. Influence of the local graphene topography

The graphene sheet is by no means a flat, perfect surface. We have already shown wrinkles that form during cooling down of a graphene flake grown by CVD on Ir(111) at elevated temperatures. These are caused by the difference of the thermal expansion coefficients of both graphene and the Iridium substrate. Upon cooling the accompanied compressive stress is relieved through the formation of wrinkles in the graphene sheet. The formation of these wrinkles and stress relieve can be tracked *in situ* with LEEM [67]. However, the wrinkles cannot lift the stress homogeneously from the graphene flakes. Locally regions with different amount of residual stress remain also below room temperature. Those regions have a slightly different lattice constant and may be differently well aligned with the underlying substrate lattice. LEEM allows to visualize this residual stress locally on a micrometer scale, due to the minute differences in the local (electronic) structure. Figure 5(a) shows a LEEM intensity versus voltage (LEEM-IV) plot measured on the two adjacent areas marked in figure 5(b). Both areas are separated by wrinkles. The data is normalized to the intensity in mirror mode, i.e., for negative start voltages. The plot of the difference of both curves reveals that the intensity in both regions differs by up to 10% for start voltages between 4–8 V. In another LEEM study, it was found that the regions with a higher intensity correspond to more relaxed graphene [67]. With this knowledge, we can thus assign the graphene sheet in region A to be in a slightly more relaxed state than that in region B, i.e., the lattice could accommodate itself more closely to the Ir(111) substrate. This is also reasonable judging from the shape of the wrinkles surrounding regions A and B: region A is rather small and surrounded by a neat hexagon of wrinkles, while region B is large and surrounded by less regular wrinkles.

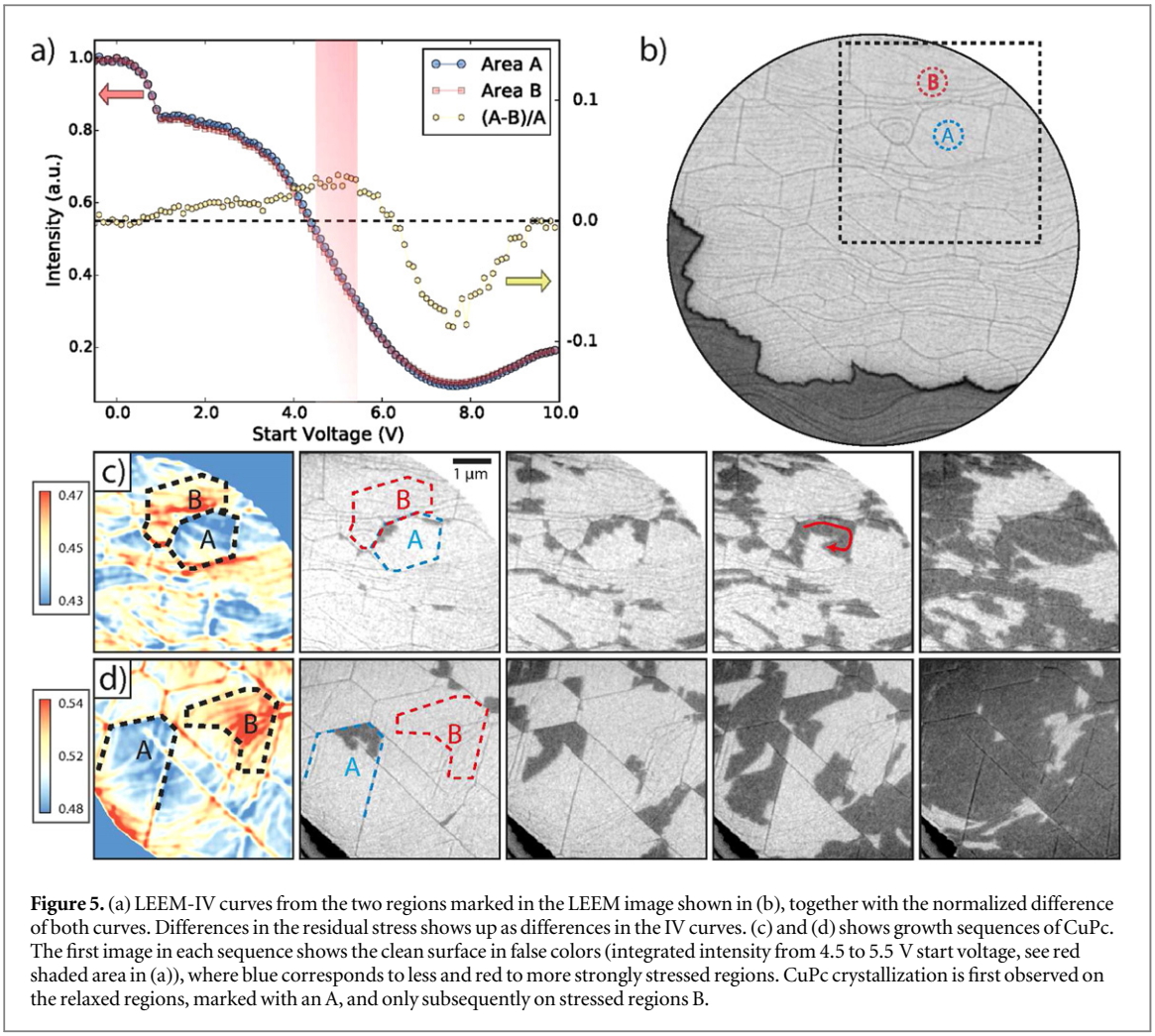

Figure 5. (a) LEEM-IV curves from the two regions marked in the LEEM image shown in (b), together with the normalized difference of both curves. Differences in the residual stress shows up as differences in the IV curves. (c) and (d) shows growth sequences of CuPc. The first image in each sequence shows the clean surface in false colors (integrated intensity from 4.5 to 5.5 V start voltage, see red shaded area in (a)), where blue corresponds to less and red to more strongly stressed regions. CuPc crystallization is first observed on the relaxed regions, marked with an A, and only subsequently on stressed regions B.

The question arises if and how this difference in the graphene topography influences the growth of the CuPc monolayer. Figures 5(c) and (d) show LEEM snapshots from two experiments of the nucleation of the crystalline CuPc phase at substrate temperatures of about 210 K (c) and 250 K (d), respectively. In both image sequences region A belongs to a more relaxed and region B to a more stressed area of the graphene sheet. The first image of each sequence shows the clean surface with its image contrast integrated over a start voltage range of 4.5–5.5 V (red shaded area in figure 5(a)) and in false colors to emphasize the difference, where blue corresponds to more relaxed, red to more stressed regions.

Both image sequences in figures 5(c) and (d) clearly show the following behavior: CuPc domains nucleate first within more relaxed regions close to wrinkles. The areas A and B in both sequences highlight examples of this, and more examples are easily found in both sequences. After nucleation, the expansion of the CuPc domains is further influenced by the distribution of the different stress levels. For instance in figure 5(c), the domain that nucleated in region A grows first along the wrinkles on the upper and right side (see red arrow), and only in the end covers the lower part, which is slightly more stressed (as can be seen in the false color image).

This effect is even more obvious, if we compare the growth of CuPc on graphene flakes of completely different orientation with respect to the Ir(111) substrate. Figure 6 shows the deposition of CuPc on a R0 graphene flake, that is surrounded by flakes of another orientation (RX, presumably a flake rotated by 30°, which is the most abundant graphene orientation besides R0 [43]). For the start voltage used (2.4 V), the R0 orientation appears bright, and flakes rotated by 14°or 30°dark[43]. This configuration, a R0 flake surrounded by RX flakes, forms due to different growth rates: while the RO variant nucleates first, the growth rates for the other graphene orientations are much higher.

The image sequence in figure 6 shows that CuPc crystals nucleate initially on the R0 domains. Once the R0 domain is almost fully covered, we also observe nucleation on the surrounding RX flake. This is consistent with the picture presented above, of preferred CuPc nucleation on the best aligned areas on the flakes.

How can we explain this preferred nucleation on the aligned graphene flakes? The main difference between the different graphene orientations is the interaction with the substrate. Aligned, R0 graphene was found to show a stronger chemisorption character on the Ir substrate than RX domains, and exhibits hybridization of the

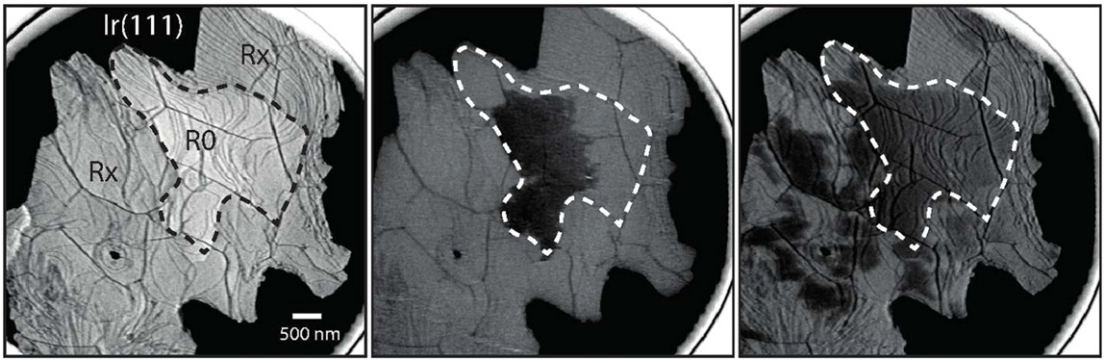

Figure 6. Deposition of CuPc on a R0 graphene flake surrounded by a rotated RX flake (most likely a flake rotated by 30°, the most abundant misaligned graphene orientation [43]). The shape of the R0 flake is marked with a dashed contour. CuPc domains (dark gray) nucleate first on the R0 domain (middle image), then on the flake with another orientation (right image).

graphene electronic bands with the Ir bands. All other graphene orientations show more physisorptive character [68]. The R0 domains also have the lowest work functions. In principle, there are three possible mechanisms, which might be responsible for the earlier nucleation:

(1) The sticking coefficient, and thus the residence time of CuPc molecules, is higher on the aligned graphene areas, possibly caused by a smaller distance of the molecules to the Ir(111) substrate. As a result, the density of molecules is higher on these areas, which induces earlier nucleation. This is a reasonable explanation, however, two observations point against it. First, the molecules do not desorb from the surface at the temperatures used here, i.e., the sticking coefficient should be close to unity on all types of graphene flakes. Second, the different graphene areas in figure 6 are separated by wrinkles, which are several nanometer high protrusions [67]. It is reasonable that these are impenetrable barriers for diffusing CuPc molecules, given that they would prefer the closer contact to the Ir(111) substrate and avoid the delaminated graphene at the wrinkles. This would mean that there is no mass exchange between both areas and the total molecular density is on average very similar everywhere.

(2) The Ir(111) influences the orientation of the molecules more strongly on the aligned graphene areas, as compared to the more misaligned areas. Obviously, the right orientation of the molecules plays a major role in the nucleation process, since the molecules are randomly oriented in the disordered phase, but show only one orientation in the crystalline phase relative to the Gr/Ir(111) substrate. Due to the substrate symmetry, this single orientation appears as a six-fold symmetry. The alignment of the orientation is caused by the interaction with the substrate, most likely the Ir(111) crystal. The electron bands of the pure R0 graphene variants are hybridized with the Ir bands [68], which makes it likely that the CuPc orientation, even in the disordered phase, is more strongly influenced on the R0 graphene. It is plausible, that stronger average alignment will result in an increased effective molecule–molecule interaction, which is a function of the molecules' relative orientation [69]. In pair potential calculations it has been shown that depending on the relative orientation of CuPc molecules, the interaction can change between attractive and repulsive [69]. If two molecules in the disordered phase meet, and they have a higher chance of being in the right orientation, this will allow nucleation at a lower density.

(3) On noble metal surfaces the interaction between molecules is strongly influenced by the interaction with the substrate [44–46, 70]. For example, on Cu(111) and Ag(111) CuPc molecules are chemisorbed and the LUMOs were found to be partially filled. On Cu(111) this results in an attractive interaction between molecules, and the formation of CuPc islands at a coverage of 0.76 ML was observed[45]. On Ag(111), on the other hand, this results in a repulsive interaction and a continuously shrinking unit cell with increasing coverage[46]. On the more inert Au(111) surface CuPc is physisorbed and no charge transfer into the molecules' LUMOs occurs[45]. A negligible interaction between molecules results in no islanding and crystallization only at higher coverages close to a monolayer. It seems plausible, that we observe the same effect here on the different graphene orientations. As already mentioned, graphene flakes/regions that are aligned w.r.t. the Ir(111) substrate (e.g. R0 flakes) show more chemisorptive character, with Ir electron bands leaking into the graphene, while all other graphene orientations show more physisorptive character. This results in different doping (misaligned graphene being p-doped), which will influence the filling of the CuPc LUMOs and in turn is known to control the molecule–molecule interaction.

An interesting question is, if the observed difference in interaction between molecules is caused by the different doping, or by the Ir(111) d-bands leaking more into the R0 graphene flakes. If it was just caused by the

doping, it should be feasible to control the crystallization of CuPc on graphene by applying a bias voltage, independent of the substrate.

5. Conclusion

To summarize, we studied the submonolayer growth of a CuPc film on Graphene/Ir(111) using *in situ* electron microscopy. Two distinct surface phases were observed: a disordered phase at low CuPc coverages and an ordered crystalline phase. The crystalline phase nucleates at relatively high coverages between 0.81 ML (220 K) and 0.92 ML (280 K). The phase transition is reversible: upon increasing the temperature the crystalline domains melt, upon decreasing the temperature they form again. Desorption of molecules from the surface is negligible below 450 K. Using dark field LEEM, we showed that individual crystalline domains could become micrometer sized, only limited by wrinkles of the graphene flakes. Graphene also forms wrinkles on other substrates including SiO_2 [71], so the same size limitation should also apply for CuPc crystallites there. The CuPc crystals show one crystal structure with six equivalent orientational domains, which is in accordance with the six-fold symmetry of the graphene and Ir(111) substrate.

The crystallization of CuPc starts first on those regions of the graphene flakes that show alignment w.r.t. the underlying Ir(111) substrate. We observed this effect on individual R0 graphene flakes, and also between flakes of completely different orientation. We explain this difference in the nucleation behavior with the different influence of the Ir(111) substrate on aligned and misaligned graphene sheets or areas. Aligned graphene is in closer contact with the Ir substrate and more chemisorbed, while all other orientations show a more physisorptive character. The experiment indicated clearly that the closer Ir substrate induces an earlier CuPc nucleation. This could be understood by an increased adsorption energy, by orientational alignment of the molecules or through doping (or a combination of these effects). Especially the last point would be interesting, it could allow to steer the nucleation by application of a bias voltage to a graphene sheet. To check this, it would be necessary to grow CuPc on graphene on another substrate with tunable doping or with the ability to apply a bias voltage, in order to exclude the influence of the Ir substrate.

References

[1] Novoselov K S, Jiang D, Schedin F, Booth T J, Khotkevich V V, Morozov S V and Geim A K 2005 *Proc. Natl Acad. Sci. USA* **102** 10451
[2] Liu W, Jackson B L, Zhu J, Miao C-Q, Chung C-H, Chung C-H, Park Y-J, Sun K, Woo J and Xie Y-H 2010 *ACS Nano* **4** 3927
[3] Hsu C-L, Lin C-T, Huang J-H, Chu C-W, Wei K-H and Li L-J 2012 *ACS Nano* **6** 5031
[4] Jang J, Park J, Nam S, Anthony J E, Kim Y, Kim K S, Kim K S, Hong B H and Park C E 2013 *Nanoscale* **5** 11094
[5] Hlawacek G, Khokhar F S, van Gastel R, Poelsema B and Teichert C 2011 *Nano Lett.* **11** 333
[6] Wu Q-h, Hong G, Ng T W and Lee S T 2012 *Appl. Phys. Lett.* **100** 161603
[7] Xiao K *et al* 2013 *J. Am. Chem. Soc.* **135** 3680
[8] Singha Roy S, Bindl D J and Arnold M S 2012 *J. Phys. Chem. Lett.* **3** 873
[9] Lu Y, Goldsmith B R, Kybert N J and Johnson A T C 2010 *Appl. Phys. Lett.* **97** 083107
[10] Schedin F, Geim A K, Morozov S V, Hill E W, Blake P, Katsnelson M I and Novoselov K S 2007 *Nat. Mater.* **6** 652
[11] Xu H *et al* 2013 *Biosens. Bioelectron.* C **50** 251
[12] Wang S, Ang P K, Wang Z, Tang A L L, Thong J T L and Loh K P 2010 *Nano Lett.* **10** 92
[13] Mann J A and Dichtel W R 2013 *J. Phys. Chem. Lett.* **4** 2649
[14] Mao H, Lu Y, Lin J and Zhong S 2013 *Prog. Surf. Sci.* **88** 132
[15] Georgakilas V, Otyepka M, Bourlinos A B, Chandra V, Kim N, Kemp K C, Hobza P, Zboril R and Kim K S 2012 *Chem. Rev.* **112** 6156
[16] Rotenberg E 2012 The electronic properties of adsorbates on graphene *Graphene Nanoelectronics* (Berlin: Springer) pp 93–134
[17] Sforzini J *et al* 2015 *Phys. Rev. Lett.* **114** 106804
[18] Avdoshenko S M, Ioffe I N, Cuniberti G, Dunsch L and Popov A A 2011 *ACS Nano* **5** 9939
[19] Coletti C, Riedl C, Lee D S, Krauss B, Patthey L, von Klitzing K, Smet J H and Starke U 2010 *Phys. Rev.* B **81** 235401
[20] Hong G, Wu Q-H, Ren J, Wang C, Zhang W and Lee S-T 2013 *Nano Today* **8** 388
[21] Hämäläinen S K, Stepanova M, Drost R, Liljeroth P, Lahtinen J and Sainio J 2012 *J. Phys. Chem.* C **116** 20433
[22] Ye W-G, Liu D, Peng X-F and Dou W-D 2013 *Chin. Phys.* B **22** 117301
[23] Scardamaglia M, Lisi S and Lizzit S 2013 *J. Phys. Chem.* B **117** 3019
[24] Ogawa Y, Niu T, Wong S L, Tsuji M, Wee A T S, Chen W and Ago H 2013 *J. Phys. Chem.* C **117** 21849
[25] Zhang H G *et al* 2011 *Phys. Rev.* B **84** 245436
[26] Scardamaglia M, Forte G, Lizzit S, Baraldi A, Lacovig P, Larciprete R, Mariani C and Betti M G 2011 *J. Nanopart. Res.* **13** 6013
[27] Hlawacek G, Khokar F S, van Gastel R, Teichert C and Poelsema B 2011 *IBM J. Res. Dev.* **55** 15:1
[28] Khokhar F S, Hlawacek G, van Gastel R, Zandvliet H J W, Teichert C and Poelsema B 2012 *Surf. Sci.* **606** 475
[29] Khokhar F S, van Gastel R and Poelsema B 2010 *Phys. Rev.* B **82** 205409
[30] Al-Mahboob A, Fujikawa Y, Sakurai T and Sadowski J T 2013 *Adv. Funct. Mater.* **23** 2653
[31] Schwarz D, van Gastel R, Zandvliet H J W and Poelsema B 2012 *Phys. Rev.* B **85** 235419
[32] Schwarz D, van Gastel R, Zandvliet H J W and Poelsema B 2012 *Phys. Rev. Lett.* **109** 016101
[33] Khokhar F S, van Gastel R, Schwarz D, Zandvliet H and Poelsema B 2011 *J. Chem. Phys.* **135** 124706
[34] Schwarz D, van Gastel R, Zandvliet H J W and Poelsema B 2013 *Phys. Rev. Lett.* **110** 076101
[35] Duden T, Thust A, Kumpf C and Tautz F S 2014 *Microsc. Microanal.* **20** 968
[36] Stadtmüller B, Henneke C, Soubatch S, Tautz F S and Kumpf C 2015 *New J. Phys.* **17** 023046

[37] Busse C et al 2011 Phys. Rev. Lett. 107 036101
[38] N'Diaye A T, Coraux J, Plasa T N, Busse C and Michely T 2008 New J. Phys. 10 043033
[39] Preobrajenski A B, Ng M L, Vinogradov A S and Mårtensson N 2008 Phys. Rev. B 78 073401
[40] Hämäläinen S K, Boneschanscher M P, Jacobse P H, Swart I, Pussi K, Moritz W, Lahtinen J, Liljeroth P and Sainio J 2013 Phys. Rev. B 88 201406
[41] Hattab H et al 2012 Nano Lett. 12 678
[42] Loginova E, Bartelt N C, Feibelman P J and McCarty K F 2009 New J. Phys. 11 063046
[43] Loginova E, Nie S, Thürmer K, Bartelt N C and McCarty K F 2009b Phys. Rev. B 80 085430
[44] Stadler C, Hansen S, Kröger I, Kumpf C and Umbach E 2009 Nat. Phys. 5 153
[45] Stadtmüller B, Kröger I, Reinert F and Kumpf C 2011 Phys. Rev. B 83 085416
[46] Kröger I et al 2010 New J. Phys. 12 083038
[47] Kröger I, Bayersdorfer P, Stadtmüller B, Kleimann C, Mercurio G, Reinert F and Kumpf C 2012 Phys. Rev. B 86 195412
[48] Poelsema B, Verheij L K and Comsa G 1983 Phys. Rev. Lett. 51 2410
[49] Poelsema B, Verheij L K and Comsa G 1982 Phys. Rev. Lett. 49 1731
[50] Poelsema B, Verheij L K and Comsa G 1985 Surf. Sci. 152-153 851
[51] de la Figuera J, Bartelt N and McCarty K 2006 Surf. Sci. 600 4062
[52] Wang S D, Dong X, Lee C S and Lee S T 2004 J. Phys. Chem. B 108 1529
[53] Yin S, Wang C, Xu B and Bai C 2002 J. Phys. Chem. B 106 9044
[54] Stadtmüller B, Gruenewald M, Peuker J, Forker R, Fritz T and Kumpf C 2014 J Phys. Chem. C 118 28592
[55] Kataoka T, Fukagawa H, Hosoumi S, Nebashi K, Sakamoto K and Ueno N 2008 Chem. Phys. Lett. 451 43
[56] Stadler C, Hansen S, Pollinger F, Kumpf C, Umbach E, Lee T-L and Zegenhagen J 2006 Phys. Rev. B 74 035404
[57] Stadtmüller B, Sueyoshi T, Kichin G, Kröger I, Soubatch S, Temirov R, Tautz F S and Kumpf C 2012 Phys. Rev. Lett. 108 106103
[58] Kleimann C, Stadtmüller B, Schröder S and Kumpf C 2014 J. Phys. Chem. C 118 52
[59] Stadtmüller B et al 2015b Phys. Rev. B 91 155433
[60] Mao J, Zhang H, Jiang Y, Pan Y, Gao M, Xiao W and Gao H-J 2009 J. Am. Chem. Soc. 131 14136
[61] Kozak J J, Brzezinski J and Rice S A 2008 J. Phys. Chem. B 112 16059
[62] Piasecki J, Szymczak P and Kozak J J 2010 J. Chem. Phys. 133 164507
[63] Alder B and Wainwright T 1962 Phys. Rev. 127 359
[64] Fernandes H C M, Arenzon J J and Levin Y 2007 J. Chem. Phys. 126 114508
[65] Mak C 2006 Phys. Rev. E 73 065104
[66] Zhao K, Bruinsma R and Mason T G 2011 Proc. Natl Acad. Sci. USA 108 2684
[67] N'Diaye A T et al 2009 New J. Phys. 11 113056
[68] Starodub E, Bostwick A, Moreschini L, Nie S, Gabaly F E, McCarty K F and Rotenberg E 2011 Phys. Rev. B 83 125428
[69] Kröger I, Stadtmüller B, Wagner C, Weiss C, Temirov R, Tautz F S and Kumpf C 2011 J. Chem. Phys. 135 234703
[70] Kröger I, Stadtmüller B, Kleimann C, Rajput P and Kumpf C 2011 Phys. Rev. B 83 195414
[71] Wang C, Liu Y, Lan L and Tan H 2013 Nanoscale 5 4454